*Pure Appl. Chem.*, Vol. 74, No. 9, pp. 1693–1706, 2002.


# Photoinduced transformations in semiconductor–metal nanocomposite assemblies*

Prashant V. Kamat‡

*Notre Dame Radiation Laboratory, Notre Dame, IN 46556-0579, USA*

*Abstract*: Semiconductor–metal nanocomposites provide a simple and convenient way to tailor the properties of photocatalysts. Modification of semiconductor surface improves charge separation and promotes interfacial charge-transfer processes in nanocomposite systems. Charge accumulation in the metal layer results in Fermi-level equilibration raising the quasi-Fermi level of the composite close to the conduction band level of the oxide semiconductor. Phototransformations of such composites—including morphological changes, interfacial charge-transfer processes and photocurrent generation of $TiO_2$-capped gold colloids—are presented in this review article.

## INTRODUCTION

One of the major goals behind designing semiconductor–metal composite nanoparticles is to improve the catalytic properties or to tune the luminescent or sensing properties. Contact of metal with semiconductor nanoparticles can indirectly influence the energetics and interfacial charge-transfer processes in a favorable way. Single-component semiconductor nanoparticles exhibit relatively poor photocatalytic efficiency (<5 %) since the majority of the photogenerated charge carriers undergo recombination [1,2]. Semiconductor–metal composite nanoparticles, on the other hand, facilitate charge rectification and improve the photocatalytic efficiency in these systems (Scheme 1).

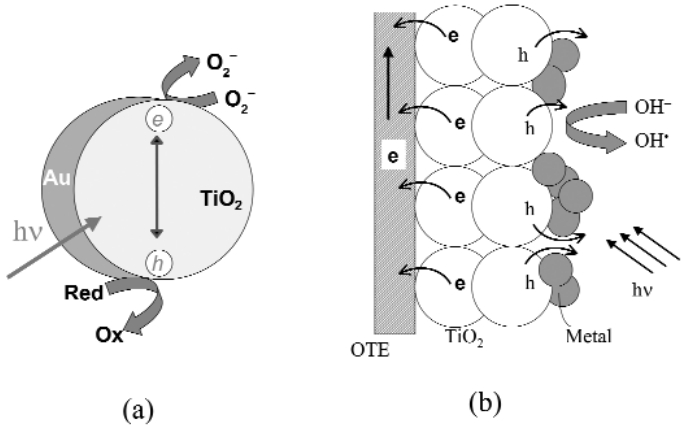


**Scheme 1** Photoinduced processes in semiconductor/metal composite nanoparticles and particulate films.

**Pure Appl. Chem.* **74**, 1489–1783 (2002). An issue of reviews and research papers based on lectures presented at the 2nd IUPAC Workshop on Advanced Materials (WAM II), Bangalore, India, 13–16 February 2002, on the theme of nanostructured advanced materials.

‡E-mail: pkamat@nd.edu; http://www.nd.edu/~pkamat

During the early years of photocatalysis, it was shown that the photoinduced deposition of noble metals such as Pt or Au on semiconductor nanoclusters enhance their photocatalytic activity [3–8]. The noble metal (e.g., Pt), which acts as a sink for photoinduced charge carriers, promotes interfacial charge-transfer processes. A direct correlation between the work function of the metal and the photocatalytic activity for the generation of $NH_3$ from azide ions has been made for metallized $TiO_2$ systems [9]. Composite semiconductor systems have also been shown to improve the photoconversion efficiency of dye-sensitized photochemical solar cells [10,11] and photocatalytic reactions [12–15]. For more than two decades, a number of research groups have been involved in modifying the photocatalytic properties of $TiO_2$ and other semiconductor materials using metal deposits [16–23].

Despite several efforts to synthesize semiconductor/metal composite systems [24–29], little information is available on the photodynamics of these materials. Fundamental understanding of the photoinduced interactions between a semiconductor and metal, as well as the interfacial charge-transfer process in nanocomposites, is important to elucidate the role of noble metals in semiconductor-assisted photocatalysis [30]. Recently, Halas and coworkers [31–33] have investigated the effect of an oxide core on the optical properties of gold nanoshell and chemically bound gold nanoparticles.

## COLLOIDAL SYSTEMS

### Synthesis and characterization of nanocomposites

Metijevic and coworkers have shown that a variety of surface coatings can be produced on cores of very different compositions [34–36]. They have shown that the formation of coatings on particles dispersed in liquids need not depend upon specific interfacial reactions. Amine-functionalized silica particles also provide a convenient way to attach gold nanoparticles to the silica surface [37,38].

A simple method of preparing semiconductor–metal nanocomposites involves reduction of the desired metal on preformed semiconductor nanoparticles (Scheme 2). For example, $TiO_2$/Au or $SnO_2$/Ag nanoparticles can be prepared by adding the desired amount of $HAuCl_4$ solution to the colloidal $TiO_2$ (acidic solution) or $AgNO_3$ solution to $SnO_2$ suspension (alkaline) in water while stirring vigorously. The $TiO_2$ colloids prepared in acidic medium were positively charged while $SnO_2$ colloids in alkaline medium carried a net negative surface charge. Thus, $AuCl_4^-$ and $Ag^+$ ions electrostatically bind to the $TiO_2$ and $SnO_2$ surfaces, respectively. Upon reduction with $NaBH_4$, we obtain stable $TiO_2$/Au and $SnO_2$/Ag nanocomposite particles in water. The presence of metal oxide colloid is important for achieving the stability of the suspension. Gold (or silver) reduction carried out in the absence of $TiO_2$ (or $SnO_2$) core using the same experimental procedure did not produce stable colloids.

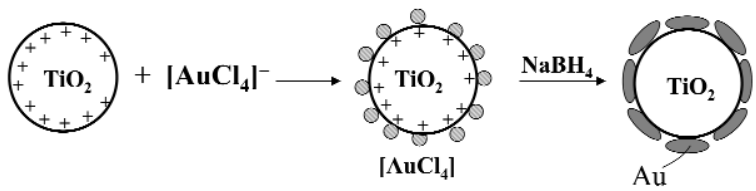


**Scheme 2** Synthesis of semiconductor/metal composite colloids.

The reduction of adsorbed ions can also be induced photocatalytically [3,39] or radiolytically [40,41]. For example, by subjecting the deaerated $TiO_2$ colloidal suspension containing $AuCl_4^-$ ions to UV light (>300 nm) for a period of 1–2 h, one can achieve capping of gold shell on $TiO_2$ nanocore. A growth in the absorption band around 520 nm (corresponding to the surface plasmon resonance) seen with increasing irradiation time confirms the formation of gold layer. The surface-adsorbed $AuCl_4^-$ ions capture the photogenerated electrons and thus get reduced at the interface. Since the interfacial electron

transfer involves a single-electron reduction, we expect the reduction of $Au^{3+}$ to $Au^0$ occurs in sequential steps ($Au^{3+} \longrightarrow Au^{2+} \longrightarrow Au^{+} \longrightarrow Au^0$). The feasibility of achieving such a stepwise reduction has been confirmed in pulse radiolysis studies [42]. A similar photocatalytic approach has been adopted to synthesize metal-capped ZnO nanoparticles [43].

The amount of core seed present in solution directly controls the size and shape of composite colloids. In the solution containing higher metal oxide core concentration [i.e., at greater ratio of $TiO_2$:Au (or $SnO_2$:Ag)], the particles are well dispersed, and a sharp and prominent absorption (spectra *a* and *c* in Fig. 1) corresponding to the surface plasmon band of the corresponding metal is observed (viz., 520 nm for Au in $TiO_2$:Au and 390 nm for Ag in $SnO_2$:Au colloids) [23]. However, for the colloids prepared using lower metal oxide concentrations [i.e., when the ratio of $TiO_2$:Au (or $SnO_2$:Ag) was kept low], we observe a dampening and broadening of the surface plasmon band and an appearance of aggregation band in the longer wavelength region (spectra *c* and *d* in Fig. 1). A red shift in the absorption maximum (405 nm) was also evident in the case of $SnO_2$:Au colloids. The lack of available charged metal oxide core at low metal oxide/metal ion ratio, disturbs the uniformity of metal ion distribution and induces aggregation effects.

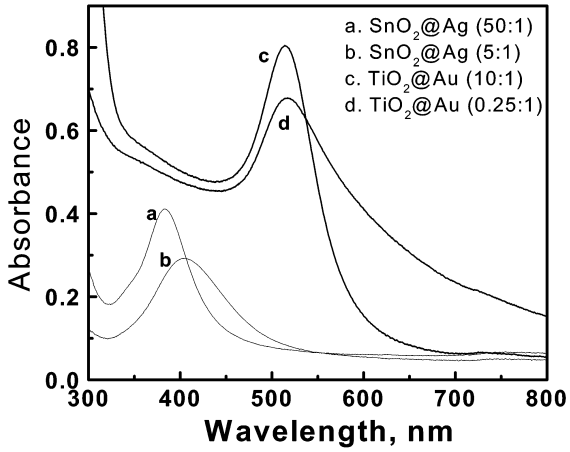


**Fig. 1** Absorption spectra of semiconductor/metal composite colloids. (From ref. [23]. Reprinted with permission from Elsevier Science.)

## Laser-induced morphological changes

$TiO_2$/Au composite nanoparticles are capable of undergoing changes under laser irradiation [23,44]. For samples with $TiO_2$:Au ratio of 20:1 and 10:1, the changes in the absorbance were relatively small. Only a small disappearance ($A < 0.03$) of the surface plasmon band was seen following a 5-min laser irradiation (532-nm excitation). Photoinduced fragmentation or dissolution of these $TiO_2$/Au nanoparticles can contribute to the small decrease in the surface plasmon band.

A more pronounced absorption change is seen when the $TiO_2$:Au nanoparticles with a ratio of 0.25:1 were subjected to laser irradiation. The difference absorption spectrum shows two distinct spectral features, viz., a bleaching in the 550–800-nm region and a growth of absorbance in the 500–550-nm region (Fig. 2). Unlike the three spectra *a–c* in Fig. 2, the absorption spectrum does not show any bleaching at 532 nm, instead an increase in the surface plasmon band with a simultaneous disappearance of the aggregation band. These observations indicate that the $TiO_2$/Au nanoparticles become isolated as the aggregates disappear following the laser pulse irradiation. The inset in Fig. 2 shows a nar-

rowing of the plasmon band at 530 nm as the colloidal $TiO_2$/Au suspension is subjected to 532-nm laser photolysis.

Figure 3 shows the transmission electron microscopy (TEM) images recorded before and after 5 min laser irradiation of an aqueous suspension of $TiO_2$/Au nanoparticles at two different core/shell

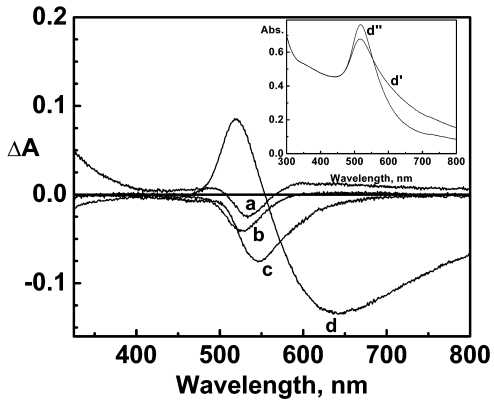


**Fig. 2** Changes in the absorption spectra of photolyzed $TiO_2$/Au nanoparticles. The absorption spectra were recorded after 5 min of laser pulse excitation (corresponding samples prior to photolysis were used as reference). The difference absorption spectra correspond to the $TiO_2$:Au ratios of (a) 20:1, (b) 10:1, (c) 1:1, and (d) 0.25:1. The inset shows the absorption spectra of $TiO_2$/Au nanoparticle ($TiO_2$:Au ratio of 0.25:1) suspension before (d′) and after (d″) laser photolysis using water as reference. (From ref. [44]. Reprinted with permission from the American Chemical Society.)

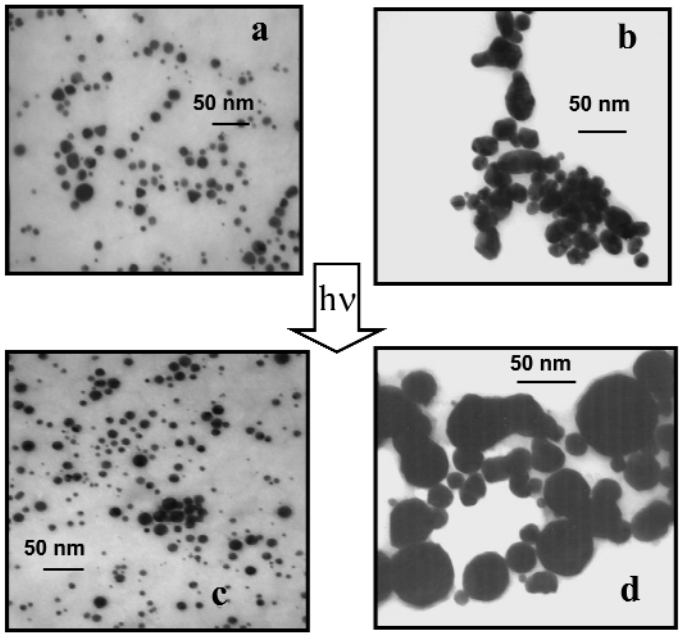


**Fig. 3** TEM images of $TiO_2$/Au nanoparticles recorded (a, b) before and (c, d) after exciting the samples with 532-nm laser pulses (10 Hz, 3 mJ/pulse) for 5 min. The ratios of $TiO_2$:Au were, (a, c) 20:1, and (b, d) 0.25:1. A growth in particle size can be seen in (d) when compared to the same sample before photolysis. (From ref. [44]. Reprinted with permission from the American Chemical Society.)

ratios. The $TiO_2$/Au samples containing high $TiO_2$:Au ratio (>1:1) exhibited remarkable stability toward laser irradiation. The TEM images did not show any major changes in the particle size or shape. Formation of a few small nanoparticles may be indicative of a photofragmentation process, but the formation occurred only to a limited extent. However, the formation of very large particles was clearly evident in the case of $TiO_2$/Au particles with a $TiO_2$:Au ratio of 0.25:1. The particles grew from 30–50 nm to 75–100 nm in diameter. An increase in the volume of 6–8 times suggests that several gold-capped $TiO_2$ nanoparticles that are in immediate contact with each other must be undergoing a fusion during the 532-nm laser pulse excitation.

As the gold particles are repeatedly bombarded with laser pulse, the temperature of these particles increases, eventually reaching melting temperature. Theoretical calculations have predicted a rise in temperatures up to 2500 K during laser excitation [45,46]. If these particles exist in the form of aggregates, the melting cluster assembly can fuse to form large size particles. In the case of larger $TiO_2$ core concentrations, the $TiO_2$/Au particles are well separated from each other, thus facilitating the heat dissipation from the particles to the surrounding aqueous medium.

Since the disappearance of the aggregation band parallels the growth of the plasmon absorption band one can follow the morphological changes by means of picosecond transient absorption spectroscopy. The linear dependence of maximum absorbance at 510 nm vs. $(\text{intensity})^2$ shows that two or more photons (532 nm) are required to induce the photofusion process in these nanoparticles [44]. Moreover, the disappearance of the aggregation band at 590 nm was found to occur with a lifetime of 0.8 ns. Thus, we can infer that the complete morphological change of $TiO_2$/Au nanoparticles occurs with an apparent rate constant of $1.25 \times 10^9$ $s^{-1}$. A recent study of melting of gold nanorods has indicated that the melting process is completed within 35 ps [47]. In our study, the longer lifetime of 0.8 ns represents the time scale required for complete morphological changes in $TiO_2$/Au core shell aggregates following the laser pulse excitation.

## Photoinduced charge separation and interparticle electron transfer

As discussed in a previous review article [2], large band-gap semiconductor nanoparticles such as $TiO_2$ and ZnO (Eg > 3.0 eV) undergo charge separation under UV excitation (reaction 1).

$$(TiO_2)\text{Au} + h\nu \rightarrow [TiO_2(e + h)]\text{Au} \quad (1)$$

While most of the charges undergo recombination, a fraction of the photogenerated electrons and holes reach the surface and participate in the redox reactions. Electron accumulation within the ZnO particle is often marked by the bleaching of exciton band [43,48,49]. If the surface of the semiconductor is capped with a metal, one can encounter storage of electrons within the metal layer, further leading to the Fermi-level equilibration.

In the case of ZnO–metal nanocomposites, the spectral changes to the surface plasmon band of the ZnO–Ag, ZnO–Au, and ZnO–Cu particles indicate substantial electron accumulation on the metal islands during photolysis [43]. Under UV irradiation electrons accumulate on the metal islands, causing a slow increase in the Fermi energy. The conduction band of bulk ZnO is located at least –0.8 V vs. NHE, significantly negative compared to the Fermi level of bulk metals (0.15 V for Ag and 0.75 V for Au). The large potential difference between the conduction band of the semiconductor and the Fermi level of the metal facilitates electron accumulation in the metal layer and shifts the apparent Fermi level close to the bottom of the conduction band. The quantized charging effects studied with organic capped gold nanoparticles suggest that the potential shift account to about 0.1 V per accumulated electron [50]. The charging of the Helmholtz and diffuse double layers at the metal shell play an important role in controlling Fermi-level equilibration [43,51]. A double-layer capacitance of 80 $\mu F/cm^2$ has been measured for Ag colloids in aqueous solution using spectroelectrochemical technique [52].

Both emission and transient absorption spectroscopy tools are convenient to probe the electron transfer between photoexcited semiconductor and metal nanostructures (Scheme 3) [21,53]. The tran-

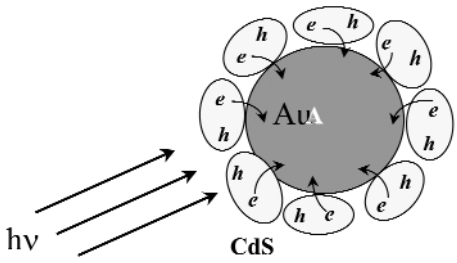


**Scheme 3** Interparticle electron transfer between CdS shell and gold nanocore.

sient absorption spectrum recorded following 355-nm laser pulse excitation of Au/CdS colloids shows two distinct transient bleaching maxima at 480 and 545 nm, which correspond to the CdS shell and Au core, respectively. The difference absorption spectrum (spectrum *c* in Fig. 4) observed in this set of experiments is compared with the individual spectra *a* and *b* (Fig. 4) recorded separately by exciting CdS and Au colloids. The photogenerated electrons in CdS nanoclusters are transferred to the Au core, causing the surface plasmon absorption to bleach. This interparticle electron transfer is completed within the laser pulse duration of 18 ps. While the surface plasmon bleaching in pristine gold colloids is seen with direct laser pulse excitation, the indirect process of electron injection mainly causes the bleaching at 545 nm in the Au/CdS composite. The former is due to heating of the electronic gas, and the latter is due to the shift in Fermi level of gold core. The situation of electron injection in the Au/CdS core is similar to the one observed during the reaction of noble metal colloids with radiolytically generated radicals [20]. The slower recovery of the transient bleaching observed in the case of Au/CdS suggested improved charge separation in the Au/CdS composite system.

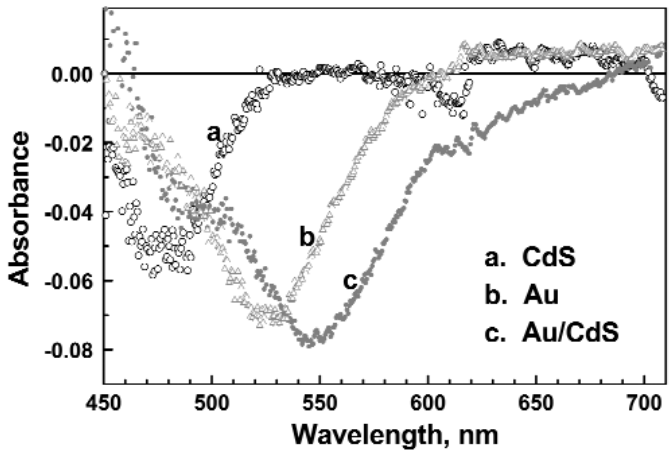


**Fig. 4** Transient absorption spectra recorded immediately after 355-nm laser pulse (pulse width 18 ps) excitation of colloidal suspension (degassed with $N_2$): (a) CdS, (b) Au and (c) Au/CdS composite. (From ref. [53]. Reprinted with permission from the American Chemical Society.)

## Photocatalytic oxidation

It has been shown that the photocatalytic electron transfer processes at the semiconductor interface can be greatly enhanced by depositing a noble metal on the semiconductor particle [18,25,54–56]. The photogenerated holes are capable of oxidizing thiocyanate ions at the semiconductor interface [57]. The

thiocyanate radicals [$(SCN)_2^{-\bullet}$] generated in the photocatalytic oxidation can be conveniently monitored from its absorbance at 480 nm [57,58].

By employing a 337-nm pulsed laser as the excitation source for exciting $TiO_2$ colloids and initiating the redox reactions at the interface, one can monitor the interfacial hole transfer process (reactions 2).

$$TiO_2(h) + SCN^- \longrightarrow TiO_2 + SCN^\bullet \text{—}(SCN^-)\rightarrow (SCN)_2^{-\bullet} \quad (2)$$

These thiocyanate radicals produced photocatalytically was found to complex with the gold surface (abs. max. 390 nm), the details of which can be found elsewhere [59].

Since the formation of $(SCN)_2^{-\bullet}$ immediately after the laser pulse excitation represents the quantitative estimate of the hole oxidation process, we monitored maximum absorbance at 480 nm at different $TiO_2$:Au ratios. (The $TiO_2$:Au ratio was varied by changing the gold concentration during sample preparation.) Figure 5 shows the dependence of $(SCN)_2^{-\bullet}$ yield on the gold shell concentration. In the absence of gold capping, $TiO_2$ colloids generate $(SCN_2)^{-\bullet}$ radicals with a quantum yield of 0.09. At low concentrations of gold, we see an increase in the efficiency of oxidation process. For a [Au]:[$TiO_2$] ratio of 0.005, we see more than 40 % enhancement in the oxidation efficiency [$\Phi(SCN)_2^{-\bullet} = 0.13$]. As we further increase the Au concentration, the efficiency of thiocyanate oxidation at gold-capped $TiO_2$ nanoparticles decreases. The inability of the photogenerated holes to reach the electrolyte interface as well as increased absorption by the gold are the likely reasons for observing lower $(SCN)_2^{-\bullet}$ yield at higher capping concentrations of gold.

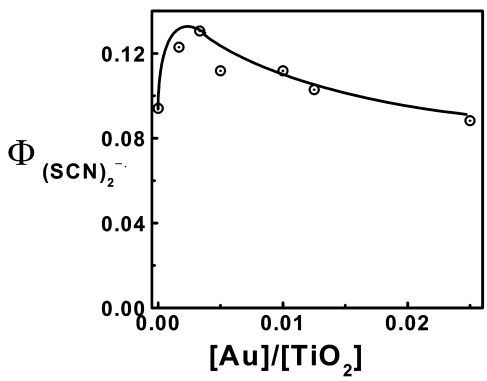


**Fig. 5** Dependence of $(SCN)_2^{-\bullet}$ yield on the concentration of gold cap. The maximum absorbance at 480 nm was used to determine the quantum yield of oxidation process using benzophenone carboxylate as actinometry reference. (From ref. [44]. Reprinted with permission from the American Chemical Society.)

On the other hand, when low concentrations of metal are used to cap the semiconductor core we can expect the outer layer to be discontinuous. Such a configuration of core-shell particles (i.e., small metal islands deposited on the $TiO_2$ core) provides a favorable geometry for facilitating the interfacial charge transfer under UV irradiation. (It should be noted that a new band appearing at 390 nm is observed in the case of $TiO_2$/Au nanoparticles as the transient absorption corresponding to $(SCN)_2^{-\bullet}$ decayed. As confirmed in our pulse radiolysis experiments [59], the 390-nm absorption band represents complexation between $(SCN)_2^{-\bullet}$ radicals and the gold surface, which further results in the oxidation of gold layer.)

## NANOSTRUCTURED FILMS

The semiconductor/metal interface achieved following sequential deposition of the two components offers many interesting scenarios. Photoelectrochemical studies [60], carried out by depositing gold nanoparticles on nanostructured $TiO_2$ films, exhibit enhanced photocurrent generation. Improved interfacial charge transfer at the semiconductor/electrolyte interface resulted in nearly three times enhancement of photocurrent generation and a shift in the apparent flat band potential. A similar decrease in the overvoltage of the interfacial charge-transfer process has been noted earlier, in semiconductor particle-assisted photocatalytic reactions [9] and *p*-GaAs single crystal-based photoelectrochemical cells [61]. Adsorption of gold nanoparticles on $TiO_2$ films as scattered islands was also found to be sufficient to induce an enhancement in the photoelectrochemical performance [60]. Local photo-current/voltage measurements have confirmed size-dependent barrier heights for the nanometal–semiconductor contacts [62].

### Preparation and characterization

Chemical, electrochemical, and photodeposition are commonly used methods to deposit noble metals on semiconductor nanoparticles. Whereas efforts have been made to bind metal nanoclusters to electrode surfaces using self-assembled monolayer [63–65] and electrophoretic [66,67] approaches, the influence of metal nanoparticles on the photoelectrochemical behavior is yet to be understood fully. Recently, we have modified nanostructured $TiO_2$ films with Au, Pt, and Ir nanoparticles using an electrophoretic approach and probed their effectiveness under photoelectrochemical and photocatalytic operation [60,67,68]. The method involved casting of $TiO_2$ films on a conducting glass electrode (referred to as optically transparent electrode, OTE) by applying colloidal $TiO_2$ suspension and annealing at 673 K. The OTE/$TiO_2$ and plain OTE electrodes were immersed in a diluted colloidal gold solution (2.5 mM Au and 20 mM TOAB in toluene) and subjected to a dc electric field of 400 V. Details of the electrophoretic deposition method can be found elsewhere [67]. The organic monolayer that surrounds the gold nanoparticle successfully suppresses interparticle interactions, and we observe surface plasmon absorption corresponding to the metal colloids. Figure 6 shows the atomic force microscopy (AFM) image of the OTE/$TiO_2$/Au composite film. The micrograph shows a porous morphology with well-separated gold nanoparticles. The electrophoretic deposition of metal nanoparticles is convenient to prepare high surface-area metal nanostructures.

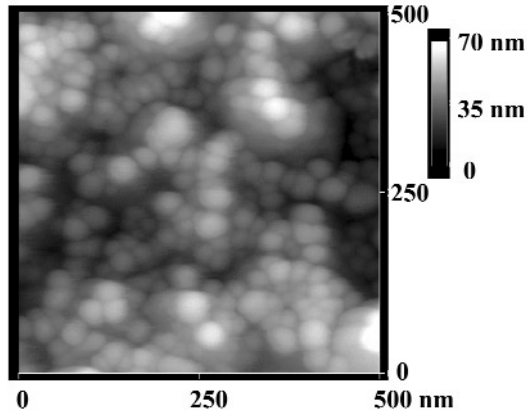


**Fig. 6** AFM image of electrophoretically deposited gold nanoparticles on an OTE/$TiO_2$ electrode. (From ref. [67]. Reprinted with permission from the American Chemical Society.)

### Improved photocurrent response

The nanostructured $TiO_2$ film cast on an OTE surface is photoactive and hence can be employed as a photoanode in a photoelectrochemical cell. The photocurrent action spectra of OTE/$TiO_2$ electrodes containing different metal nanoparticles are shown in Figure 7. The incident photon to current conversion efficiency (IPCE), defined as the number of electrons collected per incident photon, was evaluated from short-circuit photocurrent ($I_{sc}$) measurements at different wavelengths ($\lambda$) and using the expression (3),

$$\text{IPCE } \% = [1240 \times I_{sc}\,(\text{A/cm}^2)] \,/\, [\lambda\,(\text{nm}) \times I_{inc}(\text{W} \,/\, \text{cm}^2)] \times 100 \quad (3)$$

where $I_{inc}$ is the incident light power. The OTE/$TiO_2$ electrode has an onset of photocurrent around 400 nm and shows photocurrent response in the UV with an IPCE of ~5 %.

Significant enhancement in the photocurrent generation is seen upon deposition of Au, Pt, and Ir nanoparticles on the $TiO_2$ electrodes. The maximum IPCEs observed for OTE/$TiO_2$ electrodes modified with Au, Pt, and Ir particles were 28, 27, and 18 % at 300 nm, respectively. The enhancement in the photocurrent generation efficiency is indicative of the fact that the deposition of tetraoctyl ammonium bromide (TOAB)-capped metal nanoparticles is beneficial for promoting the charge separation within the nanostructured $TiO_2$ film as well as improving the interfacial charge-transfer processes. The metal nanoparticle-modified $TiO_2$ electrodes exhibit photocurrent response similar to that of unmodified $TiO_2$ films with a current onset around 400 nm. These observations indicate that the origin of the photocurrent generation lies in the band-gap excitation of $TiO_2$ film (Eg = 3.2 eV) and not in the metal.

The composite films of $TiO_2$ and Au consistently exhibit photovoltage and photocurrent greater than that of plain $TiO_2$ films, suggesting, thereby, improved charge separation in composite systems. Noble metals deposited on the semiconductor particles have been shown to improve photocatalytic electron transfer processes at the semiconductor interface [18,25,54–56]. As the hole transfer at the semiconductor/electrolyte is improved by the presence of a metal deposit we expect greater amounts of electron accumulation within the semiconductor nanocrystallites.

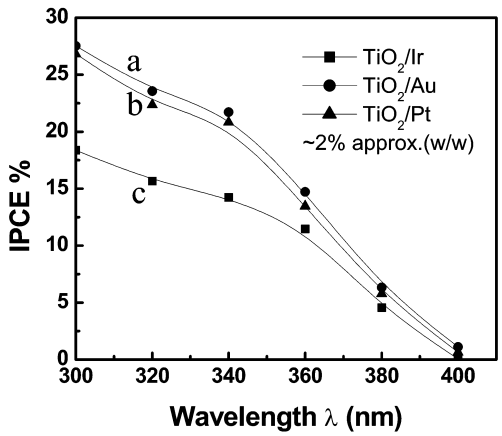


**Fig. 7** Photocurrent action spectra of OTE/$TiO_2$ electrodes modified with 3 different metal nanoparticles: (a) Au, (b) Pt, and (c) Ir. (Electrolyte: 0.05 M NaOH) (From ref. [68]. Reprinted with permission from the American Chemical Society.)

### Fermi-level equilibration

The magnitude of the photovoltage ($V_{OC}$) represents the energy difference ($\Delta E$) between the Fermi level of the $TiO_2$ film and the reduction potential of the redox couple in the electrolyte. In the dark, the Fermi

level of a semiconductor electrode equilibrates with the redox couple present in the electrolyte. As the electrons accumulate in the $TiO_2$ particulate film following the UV excitation, the pseudo-Fermi level ($E'_F$) shifts to more negative potentials, thus attaining a new photoequilibrium (Scheme 4). For an intrinsic semiconductor, we can express $E'_F$ by the expression,

$$E'_F = E_{CB} + kTln(n_c/N_c), \quad (4)$$

where $N_c$ is the effective state density and $n_c$ is the carrier density including the accumulated electrons. Any shift in $E'_F$ thus represents increased accumulation of electrons in the $TiO_2$ particulate film. While accumulation of electrons in the film is controlled by kinetic factors, the charging of the gold/TOAB nanoparticles at the interface will alter the energetics of the $TiO_2$/metal/TOAB composite film by shifting the quasi-Fermi level to more negative potentials. This scenario is illustrated in Scheme 4.

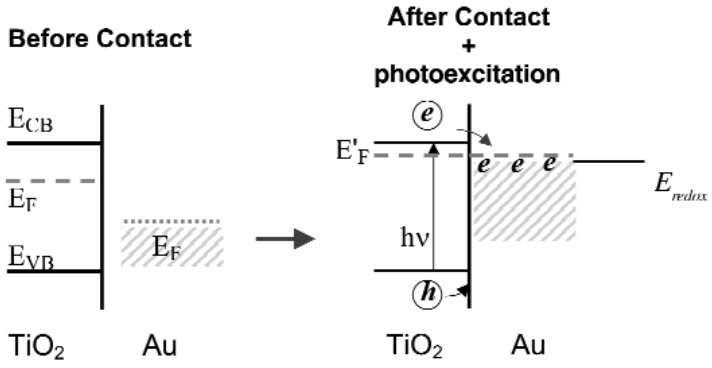


**Scheme 4** Shift in quasi-Fermi level induced by charging of Au/TOAB metal core in a $TiO_2$/Au composite film.

In order to test this we varied the redox couple in solution while monitoring the photovoltage generated at OTE/$TiO_2$ and OTE/$TiO_2$/Au electrode. Figure 8 shows the dependence of photovoltage on the reduction potential of the redox couple. With increasing reduction potential of the redox couple, we see an enhancement in the photovoltage, which is in agreement with the increasing difference between the energy levels of the semiconductor and redox couple ($\Delta V = E'_F - E^0_{redox}$). As the reduction potential increases from –0.96 V vs. SCE for anthraquinone to 1.26 V vs. SCE for thianthrene, we observe an

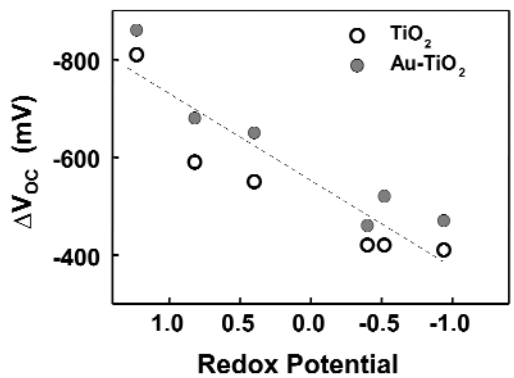


**Fig. 8** Dependence of photopotential on the reduction potential of the redox couple. The reduction potential increases from –0.96 V vs. SCE for anthraquinone to 1.26 V vs. SCE for thianthrene (see ref. [72]). The open cicrcuit photopotential corresponds to the difference between the two energy levels, viz., $E'_F - E^0_{redox}$.

increase in the $V_{OC}$ from 470 to 860 mV. Another interesting part of this experiment is the enhanced photovoltage (~150 mV) seen for the OTE/$TiO_2$/Au composite electrode. Since this increase remains almost the same for all the redox couple tested, we can conclude that the photovoltage enhancement observed for the composite film arises from the shift in the Fermi level to more negative potentials.

### Transformations during long-term photoirradiation

We have also tested the long-term stability of the $TiO_2$/Au composite films [60,67,68]. $TiO_2$-metal nanocomposite film electrodes, which initially showed an enhanced photocurrent, decayed slowly over long-term irradiation. About 50 % decrease in photocurrent was observed during 1 h of operation. (OTE/$TiO_2$ showed a smaller but steady photocurrent under the same irradiation conditions.) In these photoelectrochemical experiments, we can expect hole and/or $^{\bullet}$OH-mediated oxidation of Au nanoparticles at the $TiO_2$ interface to produce $Au^+$ ions (Scheme 5). The redox potentials of holes (+2.5 V vs. NHE) and hydroxyl radicals (+1.9 V vs. NHE) thermodynamically favor oxidation of metals such as gold [$E_{ox}$ ($Au^0/Au^+$) = 1.68 V vs. NHE]. Moreover, the gold in the nanoparticle size domain is usually more reactive than the bulk metal. Recent studies in our laboratory have shown that even mild oxidizing radicals such as $(SCN)_2^{-\bullet}$ are capable of oxidizing Au nanoparticles to produce $Au^+$ species [44,59].

Evidence exists in literature for the facile reduction of noble metal ions at irradiated $TiO_2$ nanoparticles [3,6,69–71]. While a fraction of the $Au^+$ ions might get incorporated into the $TiO_2$ matrix, the photogenerated electrons would reduce the remaining $Au^+$ ions. Thus, the $Au^+$ ions formed at the $TiO_2$/Au interface are likely to serve as recombination centers resulting in the net loss of electrons during long-term irradiation experiments (Scheme 5).

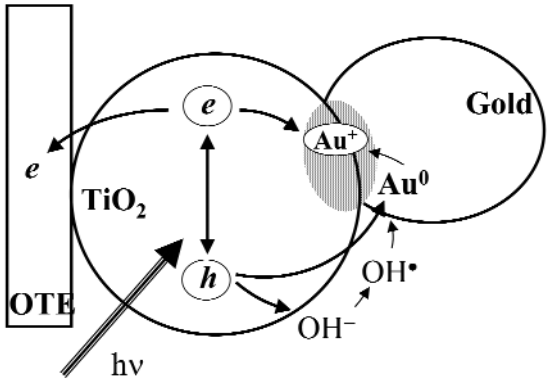


**Scheme 5** Formation of $Au^+$ at the $TiO_2$/Au interface and its possible role as recombination center.

The photocatalytic oxidation of the noble metals such as Au in composite films will not only disrupt the $TiO_2$/metal interface but will also create new electron-hole recombination centers. The contribution of these recombination centers is not significant in the short-term irradiation experiments, but continued oxidation of metal nanoparticles at long-term irradiation becomes counter-productive for the photocurrent generation. Whereas modification of the semiconductor surface with metal nanoparticles is advantageous to promote the charge-transfer process at the interface, it is important to tackle the problems associated with metal oxidation at the semiconductor/metal interface.

## CONCLUDING REMARKS

Semiconductor–metal nanocomposites provide a simple and convenient way to improve efficiency of photoinduced charge separation in a photocatalytic system. Examples of colloidal systems and nanostructured films cast on electrodes that are discussed in this review article show the usefulness of such systems in light energy conversion devices. Fermi-level equilibration achieved in the semiconductor/metal nanocomposites plays an important role in improving their photoelectrochemical and photocatalytic performance. A better understanding of the charge-transfer processes at the semiconductor/metal interface is crucial for optimizing the performance of such catalysts.

## ACKNOWLEDGMENTS

I would like to thank Dr. Nirmala Chandrasekharan, Mr. Vaidyanathan Subramanian, and Ms. Amy Dawson for the research contributions discussed in this paper. The research described herein was supported by the Office of Basic Energy Science of the Department of the Energy. This is contribution NDRL 4370 from the Notre Dame Radiation Laboratory.

## REFERENCES

1. A. J. Bard. *J. Photochem.* **10**, 59–75 (1979).
2. P. V. Kamat. *Chem. Rev.* **93**, 267–300 (1993).
3. B. Kraeutler and A. J. Bard. *J. Am. Chem. Soc.* **100**, 4317–4318 (1978).
4. A. Heller, S. E. Aharon, W. A. Bonner, B. Miller. *J. Am. Chem. Soc.* **104**, 6942–6948 (1982).
5. D. E. Aspnes and A. Heller. *J. Phys. Chem.* **87**, 4919–4929 (1983).
6. E. Borgarello, R. Harris, N. Serpone. *Nouv. J. Chim.* **9**, 743–747 (1985).
7. A. Mills and G. Williams. *J. Chem. Soc., Faraday Trans. 1* **85**, 503–519 (1989).
8. E. Amouyal and P. Koffi. *J. Photochem.* **29**, 227–242 (1985).
9. Y. Nosaka, K. Norimatsu, H. Miyama. *Chem. Phys. Lett.* **106**, 128–131 (1984).
10. C. Nasr, S. Hotchandani, W. Y. Kim, R. H. Schmehl, P. V. Kamat. *J. Phys. Chem. B* **101**, 7480–7487 (1997).
11. C. Nasr, S. Hotchandani, P. V. Kamat. *J. Phys. Chem. B* **102**, 10047–10056 (1998).
12. K. Vinodgopal and P. V. Kamat. *Environ. Sci. Technol.* **29**, 841–845 (1995).
13. K. Vinodgopal, I. Bedja, P. V. Kamat. *Chem. Mater.* **8**, 2180–2187 (1996).
14. X. Fu, L. A. Clark, Q. Yang, M. A. Anderson. *Environ. Sci. Technol.* **30**, 647–653 (1996).
15. H. Tada, T. K. Teranishi, I. Yo-ichi, S. Ito. *Langmuir* **16**, 3304–3309 (2000).
16. A. J. Bard. *J. Phys. Chem.* **86**, 172–177 (1982).
17. A. J. Bard and M. A. Fox. *Acc. Chem. Res.* **28**, 141–145 (1995).
18. A. Heller. *Pure Appl. Chem.* **58**, 1189–1192 (1986).
19. C. M. Wang, A. Heller, H. Gerischer. *J. Am. Chem. Soc.* **114**, 5230–2534 (1992).
20. A. Henglein. *J. Phys. Chem.* **97**, 5457–54571 (1993).
21. P. V. Kamat, M. de Lind, S. Hotchandani. *Isr. J. Chem.* **33**, 47–51 (1993).
22. P. Mulvaney, in *Semiconductor Nanoclusters: Physical, Chemical and Catalytic Aspects.* P. V. Kamat and D. Meisel (Eds.), pp. 99–123, Elsevier Science, Amsterdam (1997).
23. P. V. Kamat, M. Flumiani, A. Dawson. *Colloids Surf., A* **202**, 269–279 (2002).
24. P. V. Kamat. In *Semiconductor Nanoclusters: Physical, Chemical and Catalytic Aspects.* P. V. Kamat and D. Meisel (Eds.), pp. 237–259, Elsevier Science, Amsterdam (1997).
25. N. R. de Tacconi, J. Carmona, K. Rajeshwar. *J. Phys. Chem. B* **101**, 10151–10154 (1997).
26. S. H. Chen and K. Kimura. *Chem. Lett.* 233–234 (1999).
27. K. Vijaya Sarathy, P. John Thomas, G. U. Kulkarni, C. N. R. Rao. *J. Phys. Chem. B* **103**, 399–401 (1999).

28. E. P. A. M. Bakkers, E. Reitsma, J. J. Kelly, D. Vanmaekelbergh. *J. Phys. Chem. B* **103**, 2781–2788 (1999).
29. I. Pastoriza-Santos, D. S. Koktysh, A. A. Mamedov, M. Giersig, N. A. Kotov, L. M. Liz-Marzán. *Langmuir* **16**, 2731–2735 (2000).
30. P. V. Kamat. *J. Phys. Chem. B* **106**, 7729–7744 (2002).
31. R. D. Averitt, S. L. Westcott, N. J. Halas. *J. Opt. Soc. Am. B* **16**, 1824–1832 (1999).
32. S. J. Oldenburg, J. B. Jackson, S. L. Westcott, N. J. Halas. *Appl. Phys. Lett.* **75**, 2897–2899 (1999).
33. S. L. Westcott, S. J. Oldenburg, T. R. Lee, N. J. Halas. *Chem. Phys. Lett.* **300**, 651–655 (1999).
34. M. Ocana, W. P. Hsu, E. Matijevic. *Langmuir* **7**, 2911–2916 (1991).
35. H. Giesche and E. Matijevic. *J. Mater. Res.* **9**, 436 (1994).
36. V. Hardikar and E. Matijevic. *J. Colloid Interface Sci.* **221**, 133–136 (2000).
37. L. M. Liz-Marzán, M. Giersig, P. Mulvaney. *Langmuir* **12**, 4329–4335 (1996).
38. R. D. Averitt, S. L. Westcott, S. J. Oldenburg, T. R. Lee, N. J. Halas. *Langmuir* **14**, 5396–5401 (1998).
39. R. Baba, R. Konda, A. Fujishima, K. Honda. *Chem. Lett.* **10** (1986).
40. D. Lawless, S. Kapoor, P. Kennepohl, D. Meisel, N. Serpone. *J. Phys. Chem.* **98**, 9619–9625 (1994).
41. J. Belloni, M. Mostafavi, H. Remita, J. L. Marignier, M. O. Delcourt. *New J. Chem.* **22**, 1239–12555 (1998).
42. S. Mosseri, A. Henglein, E. Janata. *J. Phys. Chem.* **93**, 6791–6795 (1989).
43. A. Wood, M. Giersig, P. Mulvaney. *J. Phys. Chem. B* **105**, 8810–8815 (2001).
44. A. Dawson and P. V. Kamat. *J. Phys. Chem. B* **105**, 960–966 (2001).
45. A. Takami, H. Kurita, S. Koda. *J. Phys. Chem. B* **103**, 1226–1232 (1999).
46. H. Fujiwara, S. Yanagida, P. V. Kamat. *J. Phys. Chem. B* **103**, 2589–2591 (1999).
47. S. Link, C. Burda, B. Nikoobakht, M. A. El-Sayed. *Chem. Phys. Lett.* **315**, 12–18 (1999).
48. U. Koch, A. Fojtik, H. Weller, A. Henglein. *Chem. Phys. Lett.* **122**, 507–510 (1985).
49. G. Redmond, A. O'Keeffe, C. Burgess, C. MacHale, D. Fitzmaurice. *J. Phys. Chem.* **97**, 11081–11086 (1993).
50. S. Chen and R. W. Murray. *J. Phys. Chem. B* **103**, 9996–10000 (1999).
51. Y. Nakato, K. Ueda, H. Yano, H. Tsubomura. *J. Phys. Chem.* **92**, 2316–2324 (1988).
52. T. Ung, D. Dunstan, M. Giersig, P. Mulvaney. *Langmuir* **13**, 1773–1782 (1997).
53. B. Shanghavi and P. V. Kamat. *J. Phys. Chem. B* **101**, 7675–7679 (1997).
54. Y. Nosaka, Y. Ishizuka, H. Miyama. *Ber. Bunsenges. Phys. Chem.* **90**, 1199–204 (1986).
55. Y. Chen, Z. Wei, Y. Chen, H. Lin, Z. Hong, H. Liu, Y. Dong, C. Yu, W. Li. *J. Mol. Catal.* **21**, 275–289 (1983).
56. Y. Nakato and H. Tsubomura. *Isr. J. Chem.* **22**, 180–183 (1982).
57. P. V. Kamat. *Langmuir* **1**, 608–611 (1985).
58. D. Behar, P. L. T. Bevan, G. Scholes. *J. Phys. Chem.* **76**, 1537–1542 (1972).
59. A. Dawson and P. V. Kamat. *J. Phys. Chem. B* **104**, 11842–11846 (2000).
60. N. Chandrasekharan and P. V. Kamat. *J. Phys. Chem. B* **104**, 10851–10857 (2000).
61. A. Meier, I. Uhlendorf, D. Meissner. *Electrochim. Acta* **40**, 1523 (1995).
62. R. Hiesgen and D. Meissner. *J. Phys. Chem. B* **102**, 6549–6557 (1998).
63. D. Amihood, E. Katz, I. Willner. *Langmuir* **11**, 1313–1317 (1995).
64. V. L. Colvin, A. N. Goldstein, A. P. Alivisatos. *J. Am. Chem. Soc.* **114**, 5221–5230 (1992).
65. T. Yonezawa, H. Mutsune, T. Kunitake. *Chem. Mater.* **11**, 33–35 (1999).
66. M. Giersig and P. Mulvaney. *J. Phys. Chem.* **97**, 6334–6336 (1993).
67. N. Chandrasekharan and P. V. Kamat. *Nano Lett.* **1**, 67–70 (2001).
68. V. Subramanian, E. Wolf, P. V. Kamat. *J. Phys. Chem. B* **105**, 11439–11446 (2001).
69. B. Ohtani, Y. Okugawa, S. Nishimoto, T. Kagiya. *J. Phys. Chem.* **91**, 3550–3555 (1987).

70. J. M. Herrmann, J. Disdier, P. Pichat. *J. Catal.* **113**, 72–81 (1988).
71. W.-Y. Lin and K. Rajeshwar. *J. Electrochem. Soc.* **144**, 2751–2756 (1997).
72. G. Nagasubramanian, B. L. Wheeler, A. J. Bard. *J. Electrochem. Soc.* **130**, 1680 (1983).